journal of the mechanical behavior of biomedical materials 142 (2023) 105808

Contents lists available at ScienceDirect

Journal of the Mechanical Behavior of Biomedical Materials

journal homepage: www.elsevier.com/locate/jmbbm

Mechanical characterization of a novel biomimetic artificial disc for the cervical spine

Celien A.M. Jacobs [a], S. Amir Kamali [b], Abdelrahman M. Abdelgawad [c,d], Björn P. Meij [b], Samaneh Ghazanfari [c,d], Marianna A. Tryfonidou [b], Stefan Jockenhoevel [c,d], Keita Ito [a,*]

[a] Orthopedic Biomechanics, Dept. of Biomedical Engineering, Eindhoven University of Technology, De Rondom 70, 5612, AP, Eindhoven, the Netherlands
[b] Department of Clinical Sciences, Faculty of Veterinary Medicine, Utrecht University, Yalelaan 108, 3584, CM, Utrecht, the Netherlands
[c] Aachen-Maastricht Institute for Biobased Materials, Faculty of Science and Engineering, Maastricht University, Brightlands Chemelot Campus, Urmonderbaan, 226167, RD, Geleen, the Netherlands
[d] Department of Biohybrid and Medical Textiles (BioTex), AME – Institute of Applied Medical Engineering, Helmholtz Institute, RWTH Aachen University, Forckenbeckstraße 55, 52074, Aachen, Germany

ARTICLE INFO

Keywords:
Biomechanical
Cervical disc replacement
Biomimetic

ABSTRACT

A novel biomimetic artificial intervertebral disc (bioAID) replacement implant has been developed containing a swelling hydrogel representing the nucleus pulposus, a tensile strong fiber jacket as annulus fibrosus and titanium endplates with pins to primarily secure the device between the vertebral bodies. In this study, the design safety of this novel implant was evaluated based on several biomechanical parameters, namely compressive strength, shear-compressive strength, risk of subsidence and device expulsion as well as identifying the diurnal creep-recovery characteristics of the device.

The bioAID remained intact up to 1 kN under static axial compression and only 0.4 mm of translation was observed under a compressive shear load of 20 N. No subsidence was observed after 0.5 million cycles of sinusoidal compressive loading between 50 and 225 N. After applying 400 N in antero-posterior direction under 100 N axial compressive preload, approximately 2 mm displacement was found, being within the range of displacements reported for other commercially available cervical disc replacement devices. The diurnal creep recovery behavior of the bioAID closely resembled what has been reported for natural intervertebral discs in literature.

Overall, these results indicate that the current design can withstand (shear-compression loads and is able to remain fixed in a mechanical design resembling the vertebral bodies. Moreover, it is one of the first implants that can closely mimic the poroelastic and viscoelastic behavior of natural disc under a diurnal loading pattern.

1. Introduction

Currently, anterior cervical discectomy and fusion (ACDF) is still the golden standard to treat patients with cervical radiculopathy and myelopathy due to severely degenerated cervical discs. During ACDF, the diseased intervertebral disc is removed and replaced by a cage or allograft to restore disc height and with the aim of spinal fusion of the two adjacent vertebrae resulting in loss of mobility. The loss of motion at the treated level leads to compensatory increased motion at the adjacent levels which are hypothesized to elevate the risk of adjacent segment disease (Findlay et al., 2018; Xu et al., 2018; li Wang et al., 2020; Hilibrand et al., 1999). This has motivated the search for alternative, motion-preserving, treatments.

Similar to total hip and knee replacement preserving joint motion, cervical disc replacement (CDR) can preserve mobility of the cervical spinal unit. However, the first attempts of these artificial disc replacements still suffer from several limitations because the designs are too simplistic compared to the complex structure of the natural intervertebral disc. The disc provides motion based on deformation and exhibits viscoelastic and poroelastic behavior as a result of the osmotic pressure inside the disc, giving it its shock absorbance capacity. Most of these first-generation devices have a ball-and-socket design, consisting

* Corresponding author.
E-mail addresses: c.a.m.jacobs@tue.nl (C.A.M. Jacobs), s.a.kamali@uu.nl (S.A. Kamali), Aabdelgawad2@gmail.com (A.M. Abdelgawad), B.P.Meij@uu.nl (B.P. Meij), Samaneh.ghazanfari@maastrichtuniversity.nl (S. Ghazanfari), Tryfonidou@uu.nl (M.A. Tryfonidou), stefan.jockenhovel@maastrichtuniversity.nl, jockenhoevel@ame.rwth-aachen.de (S. Jockenhoevel), k.ito@tue.nl (K. Ito).

https://doi.org/10.1016/j.jmbbm.2023.105808
Received 26 January 2023; Received in revised form 20 March 2023; Accepted 24 March 2023
Available online 7 April 2023

of a metallic or plastic core sandwiched between two metal endplates (Staudt et al., 2018; Pham et al., 2015; Galbusera and Wilke, 2018; Derman and Zigler, 2020). In these devices, the kinematics are based on articulation where one surface can slide relative to the other with limited constraint in the range of motion. Due to the stiff materials used in these designs, very limited shock absorption is facilitated which is needed to avoid overloading of the surrounding anatomical structures. Multiple studies have confirmed that implantation of such devices altered the kinematic behavior, resulting in facet overloading and increased risk of adjacent segment disease in the long-term (Rousseau et al., 2006; Shim et al., 2007; Mo et al., 2015; Lee et al., 2011). This implies that the quality of motion might be more important than only preserving motion, probably one of the reasons why the superiority of CDR to ACDF is still under debate.

Therefore, a new generation of disc replacements have been developed in recent years that contain a viscoelastic component, such as the Bryan Disc, M6-C and Freedom (Pickett et al., 2005; Patwardhan and Havey, 2019; Benzel et al., 2011; Jacobs et al., 2020). These devices already have shown benefits compared to ball-and-socket prosthesis, such as variable COR and better replication of natural kinematics. However, none of these designs can replicate the creep and recovery behavior seen as in the natural intervertebral. Therefore, a novel disc has been developed based on the hypothesis that mimicking the structure of a natural intervertebral disc would lead to similar biomechanics and reduce the risk of altering the loading pattern of adjacent spinal units (van den Broek et al., 2012a), (van den Broek et al., 2012b). The biomimetic artificial intervertebral disc (bioAID) contains a gelatinous swelling hydrogel representing the nucleus pulposus, a tensile strong ultra-high-molecular weight polyethylene (UHMWPE) fiber jacket as annulus fibrosis and titanium endplates with pins to replicate the connection between the disc and adjacent vertebrae (Fig. 1). The design of the bioAID aims to mimic the non-linear viscoelastic behavior, osmotic intradiscal pressure and creep - relaxation behavior. A previous study has shown how the bioAID can preserve the motion at the treated and adjacent level and replicate the non-linear characteristic of an intact motion segment (Jacobs et al., 2022a).

Another unique feature of this design is that it can replicate the poroelasticity seen in a natural disc, being the fluid flow throughout the porous tissue. In the bioAID, the hydrogel core contains a negative charged backbone, resulting in a difference in ion concentration between the material and surrounding solution. This results in a Donnan osmotic pressure gradient, that attracts water into the hydrogel, giving it its osmotic swelling capacity (Žuržul et al., 2020). This osmotic swelling is restricted by the fiber jacket, resulting in a high intradiscal pressure responsible for the device's compressive strength. Due to continuous loading during the day, the bioAID will experience fluid outflow that results in a reduced disc height, while during the night, the lower loading will lead to disc height recovery.

Besides preserving motion, another goal of cervical disc replacement surgery is restoration of the disc height. It is therefore important to assess if the bioAID also preserves the disc height under diurnal loading regime and determine how similar this diurnal creep-recovery behavior is compared with a natural disc. However, mechanical performance of the design is also of importance to ensure safety before introducing it clinically and to avoid common problems associated with current disc replacements such as dislocation, migration, and subsidence. Especially since the hydrogels such as the one used in this novel design do not have a long history in orthopedic applications. Thus, the goal of this study was to evaluate the design of the bioAID based on biomechanical parameters, namely compressive strength, shear-compressive strength, risk of subsidence and device expulsion as well as identifying the diurnal creep-recovery characteristics of the device.

2. Materials and methods

2.1. Implant design

The cervical bioAID prosthesis (human size: 22 × 15.5 × 5 mm, canine size 14.5 × 13.5 × 5 mm) consists of an ionized hydrogel surrounded by a membrane and three layers of fiber jacket (Fig. 1). The hydrogel was prepared by dissolving its components in ultra-pure water (Table 1). The hydrogel consists of two monomers, 2-hydroxyethyl methacrylate (HEMA) and sodium methacrylate (NaMA). When exposed to an aqueous environment, the sodium ion (Na^{+}) of NaMA dissolves, resulting in a negatively charged polymer giving the hydrogel a fixed charged density responsible for the Donnan osmotic swelling. After dissolving the hydrogel components, a disc of polyurethane foam

Table 1
Chemical components of the HEMA-NaMA hydrogel solution.

Components of the monomer solution	Function	Mol ratio	Weight (g)
Distilled water	Solvent	0.80	35.74
Sodium methacrylate 99% (NaMA)	Monomer	0.02	5.09
2-hydroxyethyl methacrylate 97% (HEMA)	Monomer	0.18	55.2
Poly (ethylene glycol) dimethacrylate, average molecular weight 550 nM	Cross-linker	0.00001	5.75
2,2′ azobis (2-methylpropionamidine) dihydrochloride, 97%	Initiator	0.0001	0.054

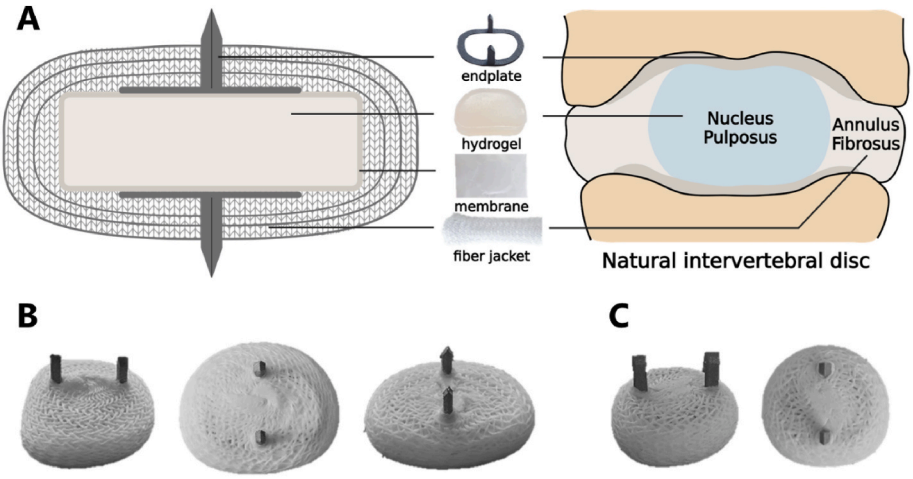

Fig. 1. A) Schematic representation (coronal plane) of the bioAID design and its mimicry to a natural intervertebral disc. B) Image of human sized bioAID. (22 × 15.5 × 5 mm) C) Image of canine sized bioAID (14 × 13 × 5 mm).

(Ø 10 × 0.2 cm, MCF.03, Corpura B.V., Etten-Leur, The Netherlands) was soaked with the hydrogel solution and polymerized under UV light (UVP XX15L, 365 nm, Analytik Jena, Upland, CA USA) for 2 h. It was subsequently heated to 45 °C for 14 h to complete polymerization. After polymerization, the hydrogel core (human size: 21 × 14.5 × 2 mm, canine size: 14 × 13 × 2 mm) was punched out. This hydrogel was sealed (thermal cutter, HSG-0, HSGM, Walluf, Germany) into a loose UHMWPE membrane pouch (38 μm thick, 5 g/m^2, 0.9 μm pore, DSM Biomedical, Geleen, the Netherlands) to contain the hydrogel. A textile tube was warp-knitted (2 × 1 lapping, 10 stitch/cm, Dept. of Biohybrid & Medical Textiles (BioTex), Helmholtz Institute Aachen, Germany) from multifilament 110 dtex UHMWPE yarn loaded with 10 wt% Hydroxy Apatite (Dyneema Purity® fiber, DSM Biomedical, Geleen, Netherlands) (Jacobs et al., 2022b). The core was then enclosed in 3 layers of this tubing and manually sewn closed with 10%HA Dyneema Purity® yarn to form an outer jacket. Before closure, a 3D printed titanium endplate ring (9 × 8 × 0.3 mm, 3D-MetalPrint, Houlle, France) with 2 mm pins was placed at the innermost layer of the jacket, such that the pins protruded out of the jacket. Before further testing, all devices were swollen in Phosphate Buffered Saline (PBS, Dulbecco's Phosphate Buffered Saline,

Sigma Aldrich) at 37 °C under a static load of 50 N, representing the weight of the human head, for 7 days to reach swelling equilibrium (Yoganandan et al., 2009).

2.2. Compression and shear-compression strength

The set-up of the static axial compression test and shear-compression test was custom-made according to the American Society for Testing and Materials (ASTM) method for static and dynamic characterization of spinal artificial disc (F2346-05) (ASTM F2346-05, 2012) and performed with a material test system (MTS; criterion model 42, MTS Systems corporation, Eden Prairie, MN USA) using a load cell of 5 kN (MTS, Model LSB.503, sensitivity of 2.227 mV/V). A motion segment was simulated via a gap between two titanium alloy (TiAL6V4) blocks (22 × 15.5 mm concave surface with 3 mm additional flat edges, 3D printed, Materialise, Leuven, Belgium) having slight concave surfaces with holes where the pins can sink in to match how the device is intended to fit between the vertebrae without considering bone ingrowth and intervertebral ligaments. Strength measurements of human sized implants (n = 5) were performed in displacement control in 37 °C PBS at a quasi-static rate of 0.001 mm/s until failure or limit of the load cell. Failure was defined as a force drop of >5% at constant displacement, or when 50% of the initial disc height was reached. Load and displacement data were continuously recorded at 10 Hz and used to calculate the stiffness, failure load, and ultimate load. Stiffness was defined as the slope of the load-displacement curve between physiological loads of 80 and 180 N, and between 180 N and the failure load. Ultimate load was defined as the maximum force the bioAID could withstand without functional failure (no drop in force).

For the shear-compression test, the testing blocks were rotated +45° in the z-axis about the y-axis such that the sample experiences a combined compression and lateral shear load (Fig. 2). To mimic bone ingrowth, the human sized implants were glued (Aquarium Munster Orca Gel Superglue) to the testing blocks and loaded in displacement mode in 37 °C PBS at a rate of 0.01 mm/s until failure, limit of the load cell or limit of the test set-up. Failure was defined as a force drop of >5%. Load and displacement data were recorded continuously at a speed of 10Hz. The displacement value at the vertical component of the shear load of 28 N (20N/cos45) was reported and should be within the range of lateral translation of the intact spine under shear loading of 2–25 N, being between 0 and 1 mm (Arshad et al., 2022). After compression and shear-compression testing, damage to the outer part of the fiber jacket, hydrogel and endplate was macroscopically inspected.

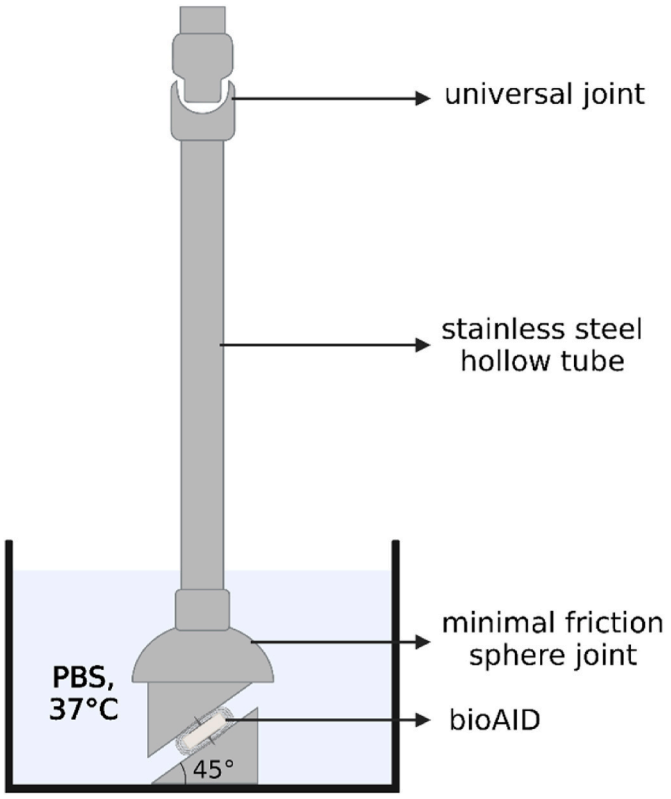

Fig. 2. Schematic representation of shear-compression test set-up based on ASTM F2346-05.

2.3. Subsidence test

Subsidence is defined as the amount of displacement the implant sinks into the adjacent vertebral bodies and its onset often occurs within the first months after implantation (Choi and Sung, 2006). Therefore, a dynamic compression testing protocol was conducted until 0.5 million cycles, representing approximately 6 months *in vivo*. It is known from literature that after 6 months osseous integration has taken place decreasing the risk of subsidence (Eijkelkamp et al., 2001). This test was performed on canine implants (n = 5) as preparation for *in vivo* study in canines. These canine implants were placed between two pieces of rigid polyurethane foam (15 × 22 × 15 mm, Sawbones®, density 0.24 g/cc, compressive modulus 4.9 MPa, Malmoë, Sweden) as defined in ASTM F1839-01 (ASTM, 2016), matching dimensions of cervical vertebrae, similar to how the device would be implanted *in vivo*. During the implantation procedure, a channel of 1 mm width and 5.5 mm depth was created in the cranial and caudal vertebrae and the keels of the bioAID endplates were inserted in ventrodorsal direction. The keels had a width of 1 mm dorsally and 1.3 mm ventrally to maximize contact surface and diminish the risk of anterior expulsion. Next, the samples were cyclically loaded in compression with sinusoidal cycles at 2 Hz between 50 and 225 N, representing physiological loads in the cervical spine (Vives-Torres et al., 2021), (Funk et al., 2011), using a MTS (Acumen Electrodynamic test system, MTS Systems corporation, loadcell 3 kN, (MTS, Model 661.18SE-02)). The amount of subsidence was assessed using a μCT scanner (CT 100, Scanco Medical, Brüttisellen, Switzerland) with an energy level of 70 kVP, intensity level of 200 μA, integration time of 200 ms and one-fold frame average. Scans were performed at high resolution mode, using a voxel size of 51 μm. CT scans were analyzed using Fiji (Schindelin et al., 2012) to identify the surface area that had less than 0.2 mm subsidence and less than 0.7 mm subsidence. First, the images were binarized, whereafter the pores in the image were filled to measure the area without taking into consideration the porous structure of the PU

foam. The percentage of non-subsided area was then calculated by dividing the area less than 0.2- or 0.7-mm depth by the total area at 2 mm depth.

2.4. Device expulsion test

Canine samples (n = 5) were used to assure safety before starting animal trials. The samples were positioned between two polyurethane foam blocks (Sawbones®, density 0.24 g/cc, compressive modulus 4.9 MPa, Malmö, Sweden) as defined in ASTM F1839-01 (ASTM, 2016), to mimic the mechanical properties of the vertebral bodies. An axial pre-load of 100 N was applied using a spring system (4 springs, C0480-045-0500, spring constant of 5.11 N/mm, Amatec, Alphen aan den Rijn, The Netherlands) to mimic the physiological axial compressive load, whereafter implants were loaded (in the dorsal to ventral direction with regard to the bioAID) with a MTS (criterion model 42, MTS Systems corporation, 500 N load cell) at a loading rate of 0.1 mm/s until 10 mm displacement or 400 N (Fig. 3). Push out load was defined as the maximum load recorded, while displacement was manually determined with a caliper to exclude plastic deformation of the sample. Video recordings were used to define the minimal push out load at which displacement started to occur.

2.5. Diurnal creep-recovery behavior

Diurnal load was simulated by 8 h at 60 N, hereafter referred to as night-loading, followed by quasi-static axial compression for 16 h at a load magnitude alternating every 30 min between 60 N and 180 N, hereafter referred to as day-loading (Fig. 4). Loading magnitudes were based on *in vivo* measurement of cervical discs in healthy human subjects performing normal neck movements (Vives-Torres et al., 2021), (Funk et al., 2011). Three diurnal loading cycles were performed, where the load-displacement values were continuously recorded at a frequency of 20 Hz. The first cycle was used as a preconditioning cycle and used to normalize measurements of cycle 2 and 3. Biomechanical parameters were calculated on the last (3rd) cycle using Matlab (MATLAB R2018b, MathWorks, Natick, MA, USA) as described in Vergroesen et al. (2018) (Vergroesen et al., 2018). The overall disc height loss was defined as the difference in height at the start of the diurnal load cycle and the end of the diurnal load cycle relative to the start of the experiment (Fig. 5). The creep during the day-loading phase is the difference in disc height at the beginning and end of the day-loading phase, while recovery is defined as the difference in disc height between the beginning and end of the night-loading phase (Fig. 5). The rate of recovery was also calculated during the second half hour of the night-loading phase (the change during the first half hour was predominantly elastic deformation) and the last half hour of the night-loading phase (Fig. 5) by determining the slope of this part of the curve. The long-term time constant was obtained by fitting the displacement data of the recovery curve to a double Voight

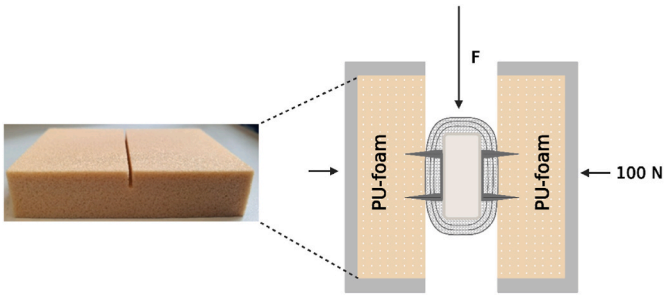

Fig. 3. Schematic representation of the bioAID expulsion set up, using polyurethane (PU) foam blocks to mimic the mechanical properties of the vertebral bodies. Push out load is depicted by F and the bioAID was axially pre-loaded by 100 N.

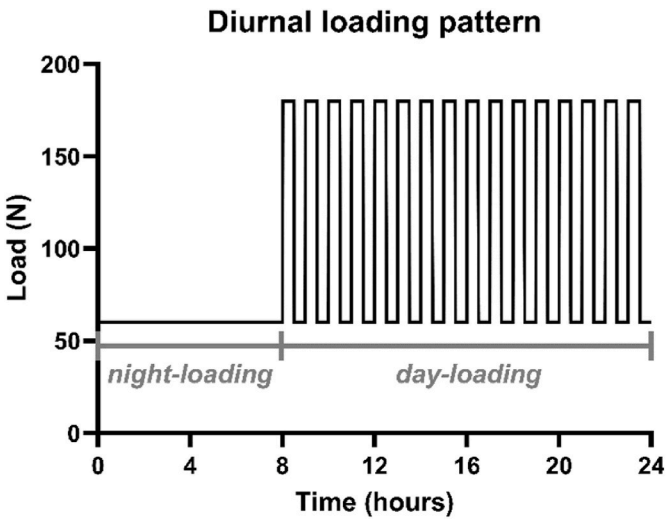

Fig. 4. One cycle of the diurnal loading pattern to evaluate the bioAID's creep-recovery behavior.

$$x(t) = L\left[\frac{1}{S_1}\left(1 - e^{-\left(\frac{t}{\tau_1}\right)}\right) + \frac{1}{S_2}\left(1 - e^{-\left(\frac{t}{\tau_2}\right)}\right) + \frac{1}{S_E}\right] \quad (1)$$

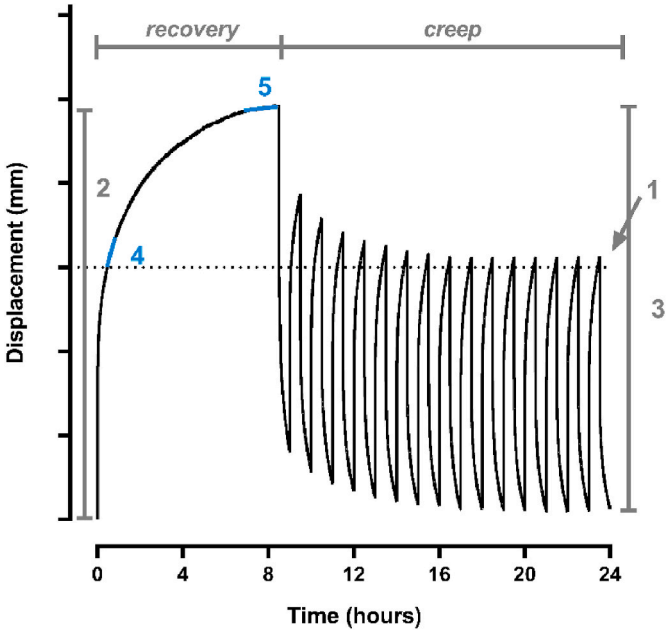

Fig. 5. Biomechanical parameters that were calculated from the diurnal creep-recovery test. 1 = overall disc height loss; 2 = recovery; 3 = creep; 4 = rate of recovery during the second half hour of the night-loading phase; 5 = rate of recovery during the last half hour of the night-loading phase.

$$FCD = \frac{m_{NaMa}\left(\frac{z_{NaMa}}{MW_{NaMA}}\right) * \frac{100\ mEq}{mol\ charge}}{m_{H_2O}} \quad (2)$$

model (Eq. (1)) using a least squares method (Van der Veen et al., 2013), where L/S_1 is the deformation of the fast Voight model at infinity, τ_1 is the time constant of the fast Voight model, L/S_2 is the deformation of the slow Voight model at infinity and τ_2 the corresponding time constant. L/S_E describes the deformation prior to the creep phase which was not

included since all parameters were calculated from the time point when the load was constant.

The water content, swelling capacity and Fixed Charged Density (FCD) were also determined by measuring the weight after production of implants (M0), after pre-load (M1), after diurnal loading cycle (M2) and after freeze-drying (Md). The water content at each timepoint was then calculated by the following formula: (M1,2 – Md), which in turn was used to calculate the FCD with Equation (2). M_{NaMA} is the mass of sodium methacrylate, Z_{NaMA} mol-charges of sodium methacrylate, MW_{NaMA} is molecular weight of sodium methacrylate and $M_{H2O}$is mass of water at each timepoint. The swelling capacity was determined by (M1,2-Md)/Md *100 to get the increase in weight in percentage.

2.6. Statistical analysis

Mean and standard deviation were calculated using Microsoft Excel. To determine differences between experimental groups, one-way ANOVA, followed by Tukey's honest post-hoc analysis was performed. Normal distribution was assessed using Shapiro-Wilk test and homogeneity of variance by Bartlett's test. A $p < 0.05$ was considered statistically significant. All statistical comparisons between groups were performed using GraphPad Prism version 8.02 for Windows (GraphPad Software). To determine the quality of the fit for the recovery results, a calculated R^2 of >0.97 was considered sufficient (MATLAB R2018b, MathWorks, Natick, MA, USA).

3. Results

3.1. Compression and shear-compression strength

The average failure load of the bioAID at 50% of the initial height of the device was 973 ± 55 N. Functional failure of the bioAID did not occur even up to 5 kN (limit of the load cell). After the test, no macroscopic failure of the jacket or membrane was observed upon disassembly. Although the hydrogel did show multiple cracks after the test, all hydrogel particles were contained within the UHMWPE membrane pouch. The average stiffness under physiological load (60–180N) was found to be 301 ± 49 N/mm (Table 2). Stiffness above physiological loads was found to be between 584 and 724 N/mm (Table 2).

Shear-compression properties of the bioAID were evaluated by reporting the amount of displacement under the 20 N shear load. The average displacement under 28 N (vertical component of lateral shear load) was 0.41 ± 0.12 mm.

3.2. Subsidence test

Fig. 6 shows the area of the polyurethane foam surface that had less than 0.2 mm or less than 0.7 mm subsidence. Approximately 10% of the surface has subsided more than 0.2 mm (Fig. 6). There was a significant difference between the cranial and caudal surfaces. Less than 1.5% of the area has a subsidence greater than 0.7 mm (Fig. 6).

3.3. Device expulsion test

Device expulsion test was performed to determine the amount of displacement in the dorsal-ventral direction under loading of 400 N, as well as the minimal force needed for device migration. After applying a dorsal-ventral load of 400 N an average displacement of 2.11 ± 0.39 mm was found. Based on the video recording, the minimum force observed to cause device migration was approximately 150 N (Fig. 7).

Table 2
Mechanical properties (mean ± SD) of the bioAID under quasi-static axial compression.

Failure load (N)	Ultimate load (kN)	Stiffness (N/mm)	
		60–180 N	180 N - failure
973 ± 55	> 5	301 ± 49	658 ± 55

3.4. Diurnal creep-recovery behavior

The poroelastic and viscoelastic properties of the bioAID under a diurnal loading pattern were evaluated. The FCD is a measure for the amount of negative charges within the hydrogel, which is dependent on the water content and thus varies throughout the diurnal loading pattern. The FCD of the bioAID during the diurnal loading pattern ranged between 0.46 ± 0.05 and 0.37 ± 0.04 mEq/g, with a corresponding swelling capacity of 64 ± 0.1 and 79 ± 0.1%.

The j-shaped creep and recovery curves show that disc height change during the day-time loading (creep) reached equilibrium, while the recovery of the disc height change during the night did not (Fig. 8). Although the recovery did not reach equilibrium, the rate of recovery decreased between the second-half hour and last-half hour of the night-loading. Moreover, the day-time creep was almost fully compensated during the recovery phase since the overall disc height loss was close to zero (Table 3). Based on the Double-Voight model, the long-term time constant of the bioAID was approximately 3 h (average R^2 of 0.99 ± 0.003) (Table 3).

4. Discussion

This study evaluated the mechanical performance of the cervical bioAID in compression, shear compression, as well as its risk for subsidence and device expulsion. Although many different loads act on the spine, the main loading direction in the spine is axial compression (Bogduk and Mercer, 2000). In the current study, the bioAID design did not fail (50% of initial height) until approximately 1 kN, being well above the estimated cervical physiological disc load of 50–150 N found in neutral posture (Arshad et al., 2022), (Moroney et al., 1988a; Barrett et al., 2020; Kumaresan et al., 2001). Although hydrogel cracks were visible after compression up to 5 kN, no functional failure and no hydrogel particles were extruded from the samples. This seems to indicate that even for peak loads, or impact loads reported to range between 100 and 1200 N the bioAID is mechanically safe (Funk et al., 2011), (Moroney et al., 1988b), (Yoganandan and Pintar, 2001). Similar to what has been found here, the compressive stiffness for a natural intervertebral disc has been reported to range between 500 and 800 N/mm when subjected to 700 N of compressive load (Yoganandan and Pintar, 2001). Stiffness within the physiological loading region is also in close agreement with previous studies, shown to range between 128 and 500 N/mm (Moroney et al., 1988b), (Yoganandan and Pintar, 2001).

Although the aim of this design concept is to replicate biomechanical properties of the native situation, comparison to existing, clinically used devices is often performed to predict clinical success. Other CDR devices have shown no failure up to 1.7–25 kN of compression (LDR Spine USA, 2001; Globus Medical, 2012; FDA 2007; NuVasive, 2012; Spinal). These devices consist mainly out of hard polymers and metals, known to have higher strength and stiffer mechanical properties (Navarro et al., 2008). Moreover, in this study, a very low strain rate of 0.001 mm/s was applied to reduce the effect of viscous dissipation, while other CDR devices were tested at much higher rates (0.2–0.4 mm/s), which can have a big effect on the failure load and stiffness of the bioAID due to its viscoelastic properties (Newell et al., 2017), (Newell et al., 2019). In general, increasing the strain rate will result in an increased stiffness and increased failure load of viscoelastic materials.

If the translation under a shear load is higher than observed for an intact disc, it will result in overloading of surrounding anatomical structures such as the facet joints (Cornaz et al., 2021), (Jaumard et al., 2011). In this study, only 0.4 mm of translation was observed under a shear load of 20 N, being within the reported range of 0–1 mm under 2–25 N (Arshad et al., 2022). Unfortunately, in this study, it was not

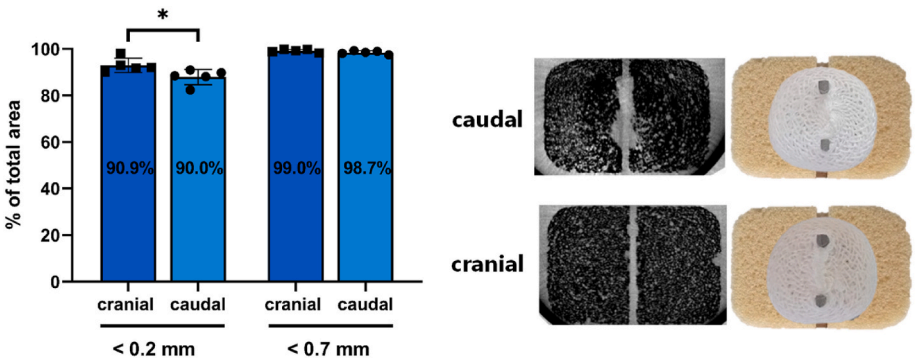

Fig. 6. Area of polyurethane foam surface (%, mean ± SD) that has less than 0.2 or less than 0.7 mm subsidence for both the cranial and caudal blocks. One way ANOVA * $p < 0.05$.

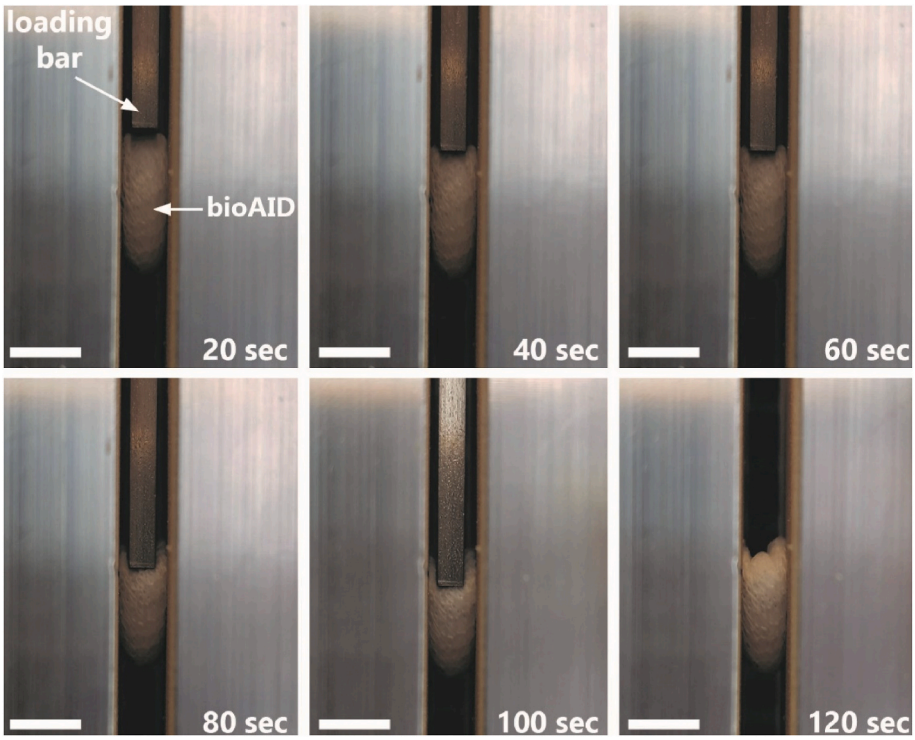

Fig. 7. Lateral view of a representative time lapse of device expulsion test showing the resistance to shear load and the plastic deformation occurring during the test. The bioAID starts to migrate after approximately 60 s which corresponds to a minimum value of 150 N in the load-displacement data. Scalebar: 7 mm.

possible to assess the ultimate compressive-shear failure and anterior-posterior shear failure of the device due to limitations in the test set-up. The maximum shear-compressive load tested here was around 100 N while maximum shear loads *in vitro* have been reported to be 135 N, and under low speed frontal impacts *in vivo* were measured between 225 and 232 N (Vives-Torres et al., 2021). A displacement of 4 mm under 20N load would correspond to approximately 50 N/mm, being at lower end of the range reported for natural intervertebral disc (78–142 N/mm) (Dowling-Medley et al., 2019). Moreover, in this study, glue was used to mimic the bone ingrowth. However, this cannot fully replicate the osseointegration, while the integration of the jacket with the bone interface will play a large role in transferring and resisting shear loads (Van Den Broek, 2012). The potential of several surface modifications to promote bone deposition was therefore assessed in a previous study (Jacobs et al., 2022b). Overall, additional research should be carried out to establish the complete failure mechanism under compressive shear loading. However, this can only be tested *in vivo*, which is currently being assessed.

To compare shear-compression results to clinically available first-generation CDR devices, first, a distinction between unconstrained and semi-constrained designs has to be made. Unconstrained implants have a variable center of rotation (COR) and allow translations in all directions, whereas semi-constrained implants have a fixed COR and only allow minimal coupled translation. Both designs are unable to resist shear in a similar fashion as a natural disc (Rousseau et al., 2006), (Yue et al., 2008). Semi-constrained designs, such as SECURE-C, Prestige LP, PCM and Mobi-C, report 2% yield loads in the range between 100 and 500 N and maximum loads of 5 kN (LDR Spine USA, 2001; Globus Medical, 2012; FDA 2007; NuVasive, 2012). This seems to indicate that these designs are extremely safe in resisting shear loading. However, *in vivo*, these more constrained designs distribute shear loads between the bone-implant interface and the facet joints, with the risk of overloading the facet joints when the implant is not properly fixated to the adjacent vertebrae. Moreover, the ability of these semi-constrained designs to distribute shear loads depends on the location of the COR, which is extremely sensitive to correct placement (Yue et al., 2008). On the other

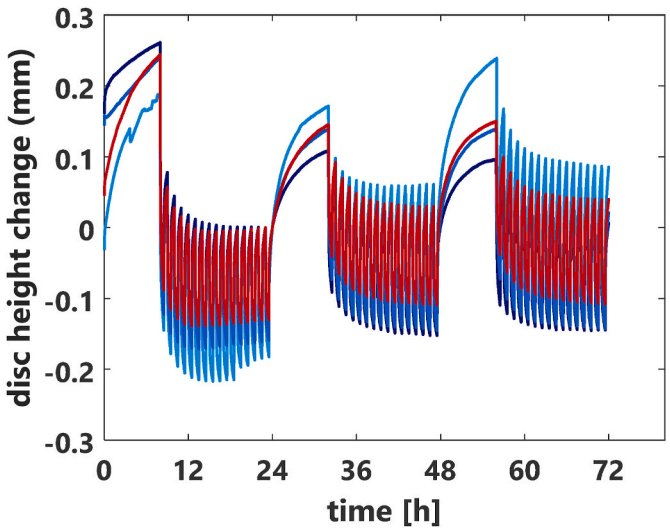

Fig. 8. Displacement data over the three diurnal cycles for each of the tested samples (each color represents a different sample). Data is normalized to the end of day 1.

Table 3
Diurnal creep - recovery characteristics of bioAID of the third cycle of diurnal loading.

overall disc height loss (mm)	Time constant (h)	rate of recovery (mm/h)		recovery (mm)	creep (mm)
		second half hour	last half hour		
0.04 ± 0.03	3.00 ± 0.35	0.05 ± 0.01	0.004 ± 0.001	0.29 ± 0.05	0.28 ± 0.04

hand, unconstrained devices, such as the Charité and DISCOVER, do not support shear loading at all, increasing the risk of developing facet arthrosis (Yue et al., 2008). Instead of solely assessing the ultimate loads under shear-compression loading, it might be valuable to also assess disc translations of CDR devices in cadavers to get more insight in the initial contact mechanism and loading of facet joints.

The results of the device expulsion and subsidence test suggest that the current design of the bioAID has a good primary stability with low risk of migration and subsidence. Based on video recordings of the device expulsion test, the minimal force needed to initiate displacement was 150 N, being above the shear load of 20 N and maximum shear load in anterior-posterior direction (equivalent to ventrodorsal direction in canines) of 135 N reported in literature (Arshad et al., 2022), (Moroney et al., 1988a). However, in extreme situations, such as those measured by Vives-Torres et al. (2021) et al., shear loads of up to 232 N have been reported (Vives-Torres et al., 2021).

After applying 400 N, approximately 2 mm displacement was found, being within the range of displacements reported for other commercially available cervical disc replacement devices (0.93 for mm Mobi-C, subluxation test 2.19 mm and core expulsion of 1.75 mm for PCM) (LDR Spine USA, 2001), (NuVasive, 2012). Average push-out loads reported for other CDR devices are within the range of 127–289 N. Unfortunately, due to differences in test set-up protocol and the limited available data, it is very difficult to compare the performance of the primary fixation with other cervical disc replacement devices. Due to the usage of 'soft' materials in the design of the bioAID, it is impossible to replicate the test analysis done on other CDR devices. Moreover, the risk of device expulsion is often increased under a certain degree of extension, which was not replicated in this test set-up. Nevertheless, the load applied in this study is 20 times higher than the shear load in the cervical spine reported in literature (White and Panjabi, 1990). This test is therefore not suitable to predict *in vivo* behavior but serves as a test scenario for assessing safety.

Risk of subsidence was assessed under 0.5 million cycles of axial compression to simulate 6 months of daily activities. It was hypothesized that the risk of subsidence is minimal after 6 months due to bone remodeling and that its risk of occurrence increases during dynamic compressive loading compared to static loading, which is most often performed to assess safety of CDR devices (LDR Spine USA, 2001), (Globus Medical, 2012), (NuVasive, 2012), (ASTM, 2014). In the current study, less than 1.5% of the surface was subsided more than the 0.7 mm threshold chosen based on the average thickness of a native human vertebral cortical endplate (Berg-Johansen et al., 2017), (Wade, 2018). This small portion of subsidence, mainly visible until 0.2 mm depth, can be attributed to the width of the keels (1 mm dorsal and 1.3 mm ventral) which are pressed into the 1 mm drilled channel of the PU foam. The difference between the cranial and caudal surface can be explained by the suture knot of the bioAID, being only present at the caudal side of the bioAID. The largest factors that increase the risk of subsidence are low bone density and footprint mismatch between the device and the surface area of the vertebral endplate (Lee, 2007; Lou et al., 2016; Thaler et al., 2013; Karaca et al., 2016). Although the PU foam does not replicate the human geometry and density distribution, the previous study has shown that the PU foam could replicate subsidence measures of middle aged human vertebrae (Au et al., 2011). To best match the geometry, the foam blocks were cut into dimensions comparable to human cervical vertebrae (Lou et al., 2016).

Assessment of the primary fixation, evaluated by the subsidence and device expulsion test, was only performed on canine implants to ensure primary stability before starting (planned) animal trials. Since only the area of the ring, and not the dimension of the keels is adjusted to match the human implants, it is expected that these results can be extrapolated to the human devices. It can therefore be assumed that the current design of the bioAID has very little subsidence risk when being implanted *in vivo*.

These standardized testing procedures are mainly used as a mechanical comparison to other CDR devices, and do not give insight into the implant's performance under *in vivo* loads and motions (ASTM F2346-05, 2012). It is often used as a measure for assuring safety after implantation. As already indicated in the previous paragraph, it is often difficult to compare the obtained data to other CDR devices due to large differences in materials, design and thus biomechanical properties. Even more challenging is that interpretation of the described method differs between studies while only limited information is reported about test conditions and results, further complicating the comparison between devices. Another aspect that hampers comparison is that each company defines its own safety threshold and testing procedure, which is often a worst-case scenario and does not predict the device's biomechanical behavior *in vivo*. Continued efforts are needed to define more physiological standardized testing methods that include safety thresholds based on data of natural discs and clinically successful CDR devices such that more biomimetic devices can be developed that potentially improve long-term risks such as adjacent segment disease. Moreover, most of the methods presented in this research determine short-term behavior of the device while the long-term durability is also of great importance. To ensure longevity, additional dynamic tests (e.g. 10–15 million cycles) under various loading regimes should be undertaken.

One of the unique features of the bioAID, is its ability to create an osmotic swelling pressure due to the negative charges of the hydrogel, giving it poroelastic properties. This poroelasticity is important for the biomechanical behavior of the bioAID, being responsible for preserving disc height and stiffness, regulating load distribution, and giving its energy absorbing and cushioning ability under axial compression. Therefore, this study also investigated the creep-recovery behavior under a diurnal loading pattern. When comparing the results of this research with data of natural intervertebral discs under a similar loading regime, it can be concluded that the bioAID can replicate a similar

pattern of the displacement – time curve (Vergroesen et al., 2018). Biomechanical parameters, such as creep, recovery, rate of recovery and overall disc height loss, were derived from this curve to be able to make a quantitative comparison with the native condition of.

The overall disc height loss was close to zero, indicating that the bioAID can fully restore the daily creep during the night. Consistent with observations for natural discs, swelling equilibrium was only reached during day-loading and not during the night-loading recovery period. Similar to *in vivo*, the disc is in a steady-state condition where swelling equilibrium is often not achieved (Cortes et al., 2014). The difference in mechanism between mechanically applied fluid outflow and pressure related fluid inflow has been proposed as a possible explanation and should be further clarified (van der Veen et al., 2005; O'Connell et al., 2011; Vergroesen et al., 2016). Moreover, during the recovery phase, the swelling is ultimately limited by tensioning of the fiber jacket, which could act as a 'sudden' stop in the transient swelling response. As hypothesized for a natural disc, the bioAID also seems to remain closer to the loading swelling equilibrium in comparison to the unloading equilibrium (Vergroesen et al., 2016). In general, fluid flow is slower towards the swelling equilibrium state, which could explain why swelling equilibrium was not reached during the night-loading compared to the day-loading (Vergroesen et al., 2016). This is also reflected in the rate of recovery, where there is a significant reduction from the second half hour compared to the last half hour. Another potential explanation for the longer time constant of the recovery phase compared to the creep phase is that permeability, and thus fluid flow, is strain dependent, which is much lower at the start of the recovery phase.

Overall, the long-term time constant for the recovery phase in this study was within the same order of magnitude as reported for a natural disc under a similar loading regime (Vergroesen et al., 2018). Within the bioAID, the fluid flow is mainly dependent on the permeability of the membrane, since the jacket has significantly larger pores (860 μm pores in the jacket vs 0.9 μm pores in the membrane). Although current results show promising similarities to the native disc, it is possible to use a membrane with either bigger or smaller pores to tune its poroelastic properties.

The absolute change of disc height of the bioAID was 0.28 mm on average, while changes in disc height for a natural disc under a similar loading pattern have been reported to be around 0.4 mm (Vergroesen et al., 2018). This is most likely related to differences in the experimental set-up, using *ex vivo* thoracolumbar goat intervertebral discs including the endplates under a dynamic testing regime in a bioreactor. Calculating the percentage of disc height change, the results seem to be more comparable, showing 6% change in this study compared to 6–10% change (assuming lumbar goat disc height of approximately 4–6 mm (Krijnen et al., 2006)) (Vergroesen et al., 2018). In literature, there is an even larger variation in reported creep for natural discs using *in vitro* test set-ups, ranging between 0.2 and 3.5 mm (Yang et al., 2022). Most of these variations arise from differences in specimen preparation, specimen species, loading regime and testing environment (Yang et al., 2022).

As previously mentioned, the FCD is responsible for the swelling pressure and dependent on the water content, which varies throughout the diurnal loading pattern, also varying the disc height. The FCD found in this study (0.37–0.46 mEq/g) is within the range of the nucleus pulposus of natural disc, known from literature to range between 0.35 and 0.6 mEq/g (Salzer et al., 2022; Sivan et al., 2014; Van Dijk et al., 2013). The water content was also comparable to what has been reported for the native situation during creep experiments (Vergroesen et al., 2018), (Paul et al., 2012). This seems to indicate that the ratio between hydroxyethyl-methacrylate and sodium-methacrylate is optimal to replicate the poroelastic behavior of the bioAID, which if needed, could be easily tuned. Nevertheless, in this research, the resultant intradiscal pressure of the bioAID and how it compares to the natural situation was not assessed. It is believed that since the FCD is within the natural range, it will also result in similar intradiscal pressure values.

5. Conclusion

Overall, these results indicate that the current design, under physiological loads, is mechanically withstanding (shear-)compression and is able to remain fixated between the vertebral bodies. Moreover, it is one of the first implants that can closely mimic the poroelastic and viscoelastic behavior of natural disc under a diurnal loading pattern.

Data and code availability

Data is available upon reasonable request.

CRediT authorship contribution statement

Celien A.M. Jacobs: Writing – review & editing, Writing – original draft, Visualization, Methodology, Investigation, Formal analysis, Data curation, Conceptualization. **S. Amir Kamali:** Writing – review & editing, Resources, Investigation. **Abdelrahman M. Abdelgawad:** Writing – review & editing, Resources, Investigation. **Björn P. Meij:** Writing – review & editing, Methodology, Investigation. **Samaneh Ghazanfari:** Writing – review & editing, Methodology, Investigation. **Marianna A. Tryfonidou:** Writing – review & editing, Supervision, Methodology, Investigation, Funding acquisition. **Stefan Jockenhoevel:** Writing – review & editing, Investigation, Funding acquisition. **Keita Ito:** Writing – review & editing, Supervision, Investigation, Funding acquisition, Conceptualization.

Declaration of competing interest

The authors declare that they have no known competing financial interests or personal relationships that could have appeared to influence the work reported in this paper.

Data availability

Data will be made available on request.

Acknowledgements

This publication is part of the project BioAID with project number 10025453 of the research program AES Open Technology Program, partly financed by the Dutch Research Council (NWO).

References

Arshad, R., Schmidt, H., El-Rich, M., Moglo, K., 2022. Sensitivity of the cervical disc loads, translations, intradiscal pressure, and muscle activity due to segmental mass, disc stiffness, and muscle strength in an upright neutral posture. Front. Bioeng. Biotechnol. 10 (April), 1–11.

ASTM, 2014. Standard test method for measuring load induced subsidence of intervertebral body fusion device under static axial compression 1," no. Reapproved 2011, 1–7.

ASTM, 2016. Standard Specification for Rigid Polyurethane Foam for Use as a Standard Material for Testing Orthopaedic Devices and Instruments, vol. 15. ASTM International, p. 6. ASTM F1839-08.

ASTM F2346-05, 2012. Standard Test Methods for Static and Dynamic Characterization of Spinal Artificial.

Au, A.G., Aiyangar, A.K., Anderson, P.A., Ploeg, H.L., 2011. A new bone surrogate model for testing interbody device subsidence. Spine (Phila. Pa. 1976 36 (16), 1289–1296.

Barrett, J.M., McKinnon, C., Callaghan, J.P., 2020. Cervical spine joint loading with neck flexion. Ergonomics 63 (1), 101–108. Jan.

Benzel, E.C., Lieberman, I.H., Ross, E.R., Linovitz, R.J., Kuras, J., Zimmers, K., 2011. Mechanical characterization of a viscoelastic disc for lumbar total disc replacement. J. Med. Dev. Trans. ASME 5 (1), 011005-1-011005–7, Mar.

Berg-Johansen, B., Fields, A.J., Liebenberg, E.C., Li, A., Lotz, J.C., 2017. Structure-function relationships at the human spinal disc-vertebra interface. J. Orthop. Res. 36 (1), 192–201. Jun.

Bogduk, N., Mercer, S., 2000. Biomechanics of the cervical spine. I : normal kinematics. Clin. Biomech. 15, 633–648.

van den Broek, P.R., Huyghe, J.M., Ito, K., van den Broek, P.R., Huyghe, J.M., Ito, K., 2012a. Biomechanical behavior of a biomimetic artificial intervertebral disc. Spine (Phila. Pa. 1976 37 (6), E367–373. Mar.

van den Broek, P.R., Huyghe, J.M., Wilson, W., Ito, K., 2012b. Design of next generation total disk replacements. J. Biomech. 45 (1), 134–140. Jan.
Choi, J.Y., Sung, K.H., 2006. Subsidence after anterior lumbar interbody fusion using paired stand-alone rectangular cages. Eur. Spine J. 15 (1), 16–22. Feb.
Cornaz, F., Widmer, J., Farshad-Amacker, N.A., Spirig, J.M., Snedeker, J.G., Farshad, M., 2021. Biomechanical contributions of spinal structures with different degrees of disc degeneration. Spine (Phila. Pa. 1976 46 (16), E869–E877.
Cortes, D.H., Jacobs, N.T., DeLucca, J.F., Elliott, D.M., 2014. Elastic, permeability and swelling properties of human intervertebral disc tissues: a benchmark for tissue engineering. J. Biomech. 47 (9), 2088–2094. Jun.
Van Den Broek, P.R., 2012. Development of a Biomimetic Artificial Intervertebral Disc. Eindhoven University of Technology.
Derman, P.B., Zigler, J.E., 2020. Cervical disc arthroplasty: rationale and history. Internet J. Spine Surg. 14 (s2), S5–S13. Aug.
Van Dijk, B.G.M., Potier, E., Ito, K., 2013. Long-term culture of bovine nucleus pulposus explants in a native environment. Spine J. 13 (4), 454–463. Apr.
Dowling-Medley, J.J., Doodkorte, R.J., Melnyk, A.D., Cripton, P.A., Oxland, T.R., 2019, 2. Shear stiffness in the lower cervical spine: Effect of sequential posterior element injury, 234, pp. 141–147. https://doi.org/10.1177/0954411919889194. Nov.
Eijkelkamp, M.F., Huyghe, J.M., van Donkelaar, C.C., van Horn, J.R., Veldhuizen, A.G., Verkerke, G.J., 2001. Requirements for an artificial intervertebral disc. Int. J. Artif. Organs 24 (5), 311–321.
FDA, 2007. Summary of safety and effectiveness data - SECURE C. U.S. Food Drug Adm 39.
Findlay, C., Ayis, S., Demetriades, A.K., 2018. Total disc replacement versus anterior cervical discectomy and fusion. Bone Jt. J. 100B (8), 991–1001. Aug.
Funk, J.R., Cormier, J.M., Bain, C.E., Guzman, H., Bonugli, E., Manoogian, S.J., 2011. Head and Neck loading in everyday and vigorous activities. Ann. Biomed. Eng. 39 (2), 766–776. Feb.
Galbusera, F., Wilke, H.-J., 2018. Chapter 18: Motion Preservation. Elsevier Ltd.
Globus Medical, I., 2012. Summary of Safety and Effectiveness Data: Prestige LP, pp. 1–18.
Hilibrand, A.S., Carlson, G.D., Palumbo, M.A., Jones, P.K., Bohlman, H.H., 1999. Radiculopathy and myelopathy at segments adjacent to the site of a previous anterior cervical arthrodesis. J. Bone Jt. Surg. - Ser. A 81 (4), 519–528. Apr.
Jacobs, C.A.M., Siepe, C.J., Ito, K., 2020. Viscoelastic cervical total disc replacement devices: design concepts. Elsevier Spine J. 20 (12), 1911–1924. Aug.
Jacobs, C.A.M., et al., 2022a. Biomechanical Evaluation of a Novel Biomimetic Artificial Intervertebral Disc in Canine Cervical Cadaveric Spines. Manuscr. Submitt. Publ.
Jacobs, C.A.M., Cramer, E.E.A., Dias, A.A., Smelt, H., Hofmann, S., Ito, K., 2022b. Surface modifications to promote the osteoconductivity of ultra-high-molecular-weight-polyethylene fabrics for a novel biomimetic artificial disc prosthesis: an in vitro study. J. Biomed. Mater. Res. Part B Appl. Biomater 1–11.
Jaumard, N.V., Welch, W.C., Winkelstein, B.A., 2011. Spinal facet joint biomechanics and mechanotransduction in normal, injury and degenerative conditions. J. Biomech. Eng. 133 (7), 071010, 1–31.
Karaca, S., Akpolat, A.O., Oztermeli, A., Erdem, M.N., Aydogan, M., 2016. Discrepancy between cervical disc prostheses and anatomical cervical dimensions. Acta Orthop. Traumatol. Turcica 50 (5), 544–547.
Krijnen, M., Mensch, D., Van Dieen, J., Wuisman, P., Smit, T., 2006. Primary spinal segment stability with a stand-alone cage: in vitro evaluation of a successful goat model. Acta Orthop. 77 (3), 454–461.
Kumaresan, S., Yoganandan, N., Pintar, F.A., Maiman, D.J., Goel, V.K., 2001. Contribution of disc degeneration to osteophyte formation in the cervical spine: a biomechanical investigation. J. Orthop. Res. 19, 977–984.
I. LDR Spine USA, "Summary of Safety and Effectiveness Data Mobi-C," 20013.
Lee, C.K., 2007. Osteopenia and total disc prosthesis subsidence: inclusion/exclusion criteria for total disc replacement. SAS J 1 (2), 82–84.
Lee, S.H., Im, Y.J., Kim, K.T., Kim, Y.H., Park, W.M., Kim, K., 2011. Comparison of cervical spine biomechanics after fixed- and mobile-core artificial sisc replacement: a finite element analysis. Spine (Phila. Pa. 1976) 36 (9), 700–708.
Lou, J., Liu, H., Rong, X., Li, H., Wang, B., Gong, Q., 2016. Geometry of inferior endplates of the cervical spine. Clin. Neurol. Neurosurg. 142, 132–136.
Mo, Z., Zhao, Y., Du, C., Sun, Y., Zhang, M., Fan, Y., 2015. Does location of rotation center in artificial disc affect cervical biomechanics? Spine (Phila. Pa. 1976 40 (8), E469–E475.
Moroney, S.P., Schultz, A.B., Miller, J.A.A., 1988a. Analysis and measurement of neck loads. J. Orthop. Res. 6 (5), 713–720. Sep.
Moroney, S.P., Schultz, A.B., Miller, A.A.J., Andersson, G.B.J., 1988b. Load-displacement properties of lower cervical spine motion segments. J. Biomech. 21 (9), 769–779.
Navarro, M., Michiardi, A., Castaño, O., Planell, J.A., 2008. Biomaterials in orthopaedics. The Royal Society J. R. Soc. Interface 5 (27), 1137–1158, 06-Oct.
Newell, N., Grigoriadis, G., Christou, A., Carpanen, D., Masouros, S.D., 2017. Material properties of bovine intervertebral discs across strain rates. J. Mech. Behav. Biomed. Mater. 65, 824–830. June 2016.
Newell, N., Carpanen, D., Grigoriadis, G., Little, J.P., Masouros, S.D., 2019. Material properties of human lumbar intervertebral discs across strain rates. Spine J. 19 (12), 2013–2024.
NuVasive, 2012. Summary of Safety and Effectivness Data: PCM.
O'Connell, G.D., Jacobs, N.T., Sen, S., Vresilovic, E.J., Elliott, D.M., 2011. Axial creep loading and unloaded recovery of the human intervertebral disc and the effect of degeneration. J. Mech. Behav. Biomed. Mater. 4 (7), 933–942. Oct.
Patwardhan, A.G., Havey, R.M., 2019. Prosthesis design influences segmental contribution to total cervical motion after cervical disc arthroplasty. Eur. Spine J. 29, 2713–2721. Jul. https://doi.org/10.1007/s00586-019-06064-4.
Paul, C.P.L., et al., 2012. Simulated-physiological loading conditions preserve biological and mechanical properties of caprine lumbar intervertebral discs in EX vivo culture. PLoS One 7 (3), e33147. Mar.
Pham, M.H., Mehta, V.A., Tuchman, A., Hsieh, P.C., 2015. Material science in cervical total disc replacement. In: BioMed Research International. Hindawi Limited, 2015.
Pickett, G.E., Rouleau, J.P., Duggal, N., 2005. Kinematic analysis of the cervical spine following implantation of an artificial cervical disc. Spine (Phila. Pa. 1976) 30 (17), 1949–1954.
Rousseau, M.A., Bradford, D.S., Bertagnoli, R., Hu, S.S., Lotz, J.C., 2006. Disc arthroplasty design influences intervertebral kinematics and facet forces. Spine J. 6, 258–266.
Salzer, E., Mouser, V.H.M., Tryfonidou, M.A., Ito, K., 2022. A bovine nucleus pulposus explant culture model. J. Orthop. Res. 40 (9), 2089–2102.
Schindelin, J., et al., 2012. Fiji: an open-source platform for biological-image analysis. Nat. Methods 9 (7), 676–682. Jun.
Shim, C.S., et al., 2007. CHARITI versus ProDisc: a comparative study of a minimum 3-year follow-up. Spine (Phila. Pa. 1976 32 (9), 1012–1018.
Sivan, S.S., et al., 2014. Injectable hydrogels with high fixed charge density and swelling pressure for nucleus pulposus repair: biomimetic glycosaminoglycan analogues. Acta Biomater. 10 (3), 1124–1133.
I. Spinal Kinetics, "Summary of Safety and Effectiveness Data M6-C.".
Staudt, M.D., Das, K., Duggal, N., 2018. Does design matter? Cervical disc replacements under review. Neurosurg. Rev. 41 (2), 399–407. Apr.
Thaler, M., Hartmann, S., Gstöttner, M., Lechner, R., Gabl, M., Bach, C., 2013. Footprint mismatch in total cervical disc arthroplasty. Eur. Spine J. 22 (4), 759–765.
van der Veen, A.J., Mullender, M., Smit, T.H., Kingma, I., van Dieën, J.H., 2005. Flow-related mechanics of the intervertebral disc: the validity of an in vitro model. Spine (Phila. Pa. 1976 30 (18), 534–539.
Van der Veen, A.J., Bisschop, A., Mullender, M.G., van Dieën, J.H., 2013. Modelling creep behaviour of the human intervertebral disc. J. Biomech. 46 (12), 2101–2103. Aug.
Vergroesen, P.P.A., van der Veen, A.J., Emanuel, K.S., van Dieën, J.H., Smit, T.H., 2016. The poro-elastic behaviour of the intervertebral disc: a new perspective on diurnal fluid flow. J. Biomech. 49 (6), 857–863. Apr.
Vergroesen, P.P.A., Emanuel, K.S., Peeters, M., Kingma, I., Smit, T.H., 2018. Are axial intervertebral disc biomechanics determined by osmosis? J. Biomech. 70, 4–9. Mar.
Vives-Torres, C.M., et al., 2021. Comparison of upper neck loading in young adult and elderly volunteers during low speed frontal impacts. Front. Bioeng. Biotechnol. 9, 682974.
Wade, K., 2018. Chapter 8 - Vertebral Endplates. Elsevier Ltd.
li Wang, Q., et al., 2020. Long-term results comparing cervical disc arthroplasty to anterior cervical discectomy and fusion: a systematic review and meta-analysis of randomized controlled trials. Orthop. Surg. 12 (1), 16–30. Feb.
White, A., Panjabi, M., 1990. Clinical Biomechanics of the Spine, second ed. Lip pincott Company, London.
Xu, S., Liang, Y., Zhu, Z., Qian, Y., Liu, H., 2018. Adjacent segment degeneration or disease after cervical total disc replacement: a meta-analysis of randomized controlled trials. J. Orthop. Surg. Res. 13 (1). J Orthop Surg Res, 03-Oct.
Yang, M., Xiang, D., Wang, S., Liu, W., 2022. In vitro studies for investigating creep of intervertebral discs under axial compression: a review of testing environment and results. Multidisciplinary Digital Publishing Institute (MDPI). Materials 15 (7), 2500, 28-Mar.
Yoganandan, S. Kumaresan, Pintar, F.A., 2001. Biomechanics of the cervical spine Part 2. Cervical spine soft tissue responses and biomechanical modeling. Clin. Biomech. 16 (1), 1–27.
Yoganandan, N., Pintar, F.A., Zhang, J., Baisden, J.L., 2009. Physical properties of the human head: mass, center of gravity and moment of inertia. J. Biomech. 42 (9), 1177–1192. Jun.
Yue, J.J., Bertagnoli, R., McAfee, P.C., An, H.S., 2008. Motion preservation surgery of the spine: advanced techniques and controversies. Am. J. Neuroradiol. 30 (9). E134–E134, Oct.
Žuržul, N., Ilseng, A., Prot, V.E., Sveinsson, H.M., Skallerud, B.H., Stokke, B.T., 2020. Donnan contribution and specific ion effects in swelling of cationic hydrogels are additive: combined high-resolution experiments and finite element modeling. Gels 6 (3), 1–20.